

## Get Clarity On Generics

Cost-Effective CT & MRI Contrast Agents

 FRESENIUS  
KABI

WATCH VIDEO

# AJNR

### Vestibular Implant Imaging

A. Hedjoudje, D.P. Schoo, B.K. Ward, J.P. Carey, C.C. Della Santina and M. Pearl

*AJNR Am J Neuroradiol* published online 24 December 2020

<http://www.ajnr.org/content/early/2020/12/24/ajnr.A6991>

This information is current as of August 5, 2025.

# Vestibular Implant Imaging

 A. Hedjoudje,  D.P. Schoo,  B.K. Ward,  J.P. Carey,  C.C. Della Santina, and  M. Pearl



## ABSTRACT

**SUMMARY:** Analogous to hearing restoration via cochlear implants, vestibular function could be restored via vestibular implants that electrically stimulate vestibular nerve branches to encode head motion. This study presents the technical feasibility and first imaging results of CT for vestibular implants in 8 participants of the first-in-human Multichannel Vestibular Implant Early Feasibility Study. Imaging characteristics of 8 participants (3 men, 5 women; median age, 59.5 years; range, 51–66 years) implanted with a Multichannel Vestibular Implant System who underwent a postimplantation multislice CT ( $n = 2$ ) or flat panel CT ( $n = 6$ ) are reported. The device comprises 9 platinum electrodes inserted into the ampullae of the 3 semicircular canals and 1 reference electrode inserted in the common crus. Electrode insertion site, positions, length and angle of insertion, and number of artifacts were assessed. Individual electrode contacts were barely discernible in the 2 participants imaged using multislice CT. Electrode and osseous structures were detectable but blurred so that only 12 of the 18 stimulating electrode contacts could be individually identified. Flat panel CT could identify all 10 electrode contacts in all 6 participants. The median reference electrode insertion depth angle was  $9^\circ$  (range,  $-57.5^\circ$  to  $45^\circ$ ), and the median reference electrode insertion length was 42 mm (range,  $-21$ –66 mm). Flat panel CT of vestibular implants produces higher-resolution images with fewer artifacts than multidetector row CT, allowing visualization of individual electrode contacts and quantification of their locations relative to vestibular semicircular canals and ampullae. As multichannel vestibular implant imaging improves, so will our understanding of the relationship between electrode placement and vestibular performance.

**ABBREVIATIONS:** FF = full-field; FPCT = flat panel CT; HR = high-resolution; MSCT = multislice CT; SCC = semicircular canal; MVI = Multichannel Vestibular Implant System

Although individuals with a unilateral vestibular deficit and 1 normal labyrinth usually compensate well via rehabilitation exercises and adaptation, those with bilateral vestibular hypofunction often have degraded visual acuity during head movement, postural instability, and chronic disequilibrium.<sup>1–3</sup> When bilateral vestibular hypofunction results from ototoxic drug exposure, Ménière disease, genetic defects, or other inner ear dysfunction sparing the vestibular nerve and central pathways, an

implantable neuroelectronic prosthesis that measures 3D head rotation and stimulates the vestibular nerve with motion-modulated electrical pulse trains could substantially improve quality of life.<sup>4,5</sup>


Vestibular implants are similar to commercially available cochlear implants in that they include an external unit that powers and communicates with an implanted inner ear stimulator via a transcutaneous inductive link.<sup>4,5</sup> The external unit includes a head-worn unit (for sensing head motion and delivering power and signals to the implanted stimulator) and a power and control unit containing a battery and microprocessor. As in cochlear implant systems, the head-worn unit and implanted stimulator each contain at least 1 magnet to hold the head-worn unit on the scalp over the implant. Unlike cochlear implant systems, vestibular implant systems sometimes include  $\geq 1$  additional magnet on each component to facilitate retention of the head-worn unit. Vestibular implant electrode arrays typically are much smaller than cochlear implant electrode arrays and are implanted in the semicircular canal (SCCs) near the ampullae, where the vestibular nerves terminate.<sup>4</sup> Variations on this approach have included an

Received May 30, 2020; accepted after revision September 10.

From the Department of Otolaryngology–Head and Neck Surgery (A.H., D.P.S., B.K.W., J.P.C., C.C.D.S.), Division of Interventional Neuroradiology (A.H., M.P.), and Department of Biomedical Engineering (C.C.D.S.), Johns Hopkins University School of Medicine, Baltimore, Maryland; Neuroradiology Unit (A.H.), Service of Diagnostic and Interventional Imaging, Sion Hospital, Sion, Valais, Switzerland; and Labyrinth Devices (C.C.D.S.), Baltimore, Maryland.

This work was supported by the National Institute on Deafness and Other Communication Disorders R01DC013536 and 2T32DC000023, Labyrinth Devices, and MED-EL.

Please address correspondence to Abderrahmane Hedjoudje, MD, MSE, Department of Interventional Neuroradiology, Johns Hopkins School of Medicine, 601 North Caroline St, Suite 6253, Baltimore, MD 21287; e-mail: ahedjou1@jhmi.edu

 Indicates open access to non-subscribers at [www.ajnr.org](http://www.ajnr.org)

<http://dx.doi.org/10.3174/ajnr.A6991>

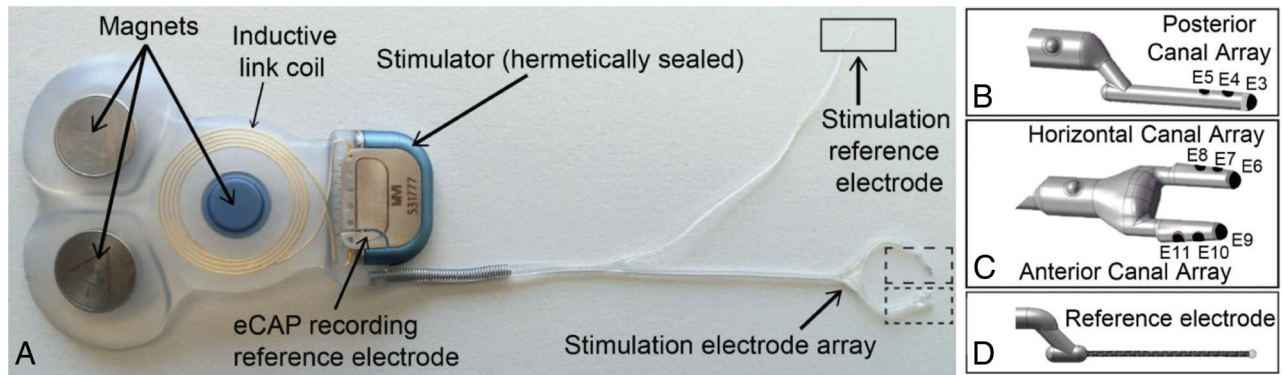


**FIG 1.** A, The MVI stimulator comprises 3 fixation magnets, an inductive coil link, electrical current stimulator circuitry, a stimulation electrode array, a stimulation reference electrode, and a recording reference electrode. The electrode array includes a 3-electrode shank for the posterior canal (B, E3–E5), a forked subarray with 2 shanks for the horizontal (C, E6–E8) and anterior (C, E9–E11) canals, and a stimulation reference electrode (D). eCAP indicates electrically evoked compound action potential. Reprinted with permission from Labyrinth Devices, LLC, 2019.

extraluminal approach (in which the surgeon attempts to expose and place electrodes near vestibular nerve branches in the distal-most aspect of the internal auditory canal and singular nerve canal); implantation of electrode arrays near the utricle and sacule; simultaneous or delayed placement of a separate electrode array in the cochlea; and variations in location of the stimulation reference electrode, which can be implanted in the labyrinth or a subperiosteal pocket (as an alternative surgical procedure) or integrated with the stimulator housing.

Empiric studies in animals and finite element models of current flow in the labyrinth indicate that electrode distances to target and nontarget nerve branches are key determinants of the strength and selectivity of stimulation. Therefore, precise knowledge of electrode location, as provided by high-resolution postoperative imaging, can provide information helpful for both prognosis and guiding the choice of which electrodes to activate and which stimulus parameters to use. Postoperative imaging performed as a part of a vestibular implant operation is useful to confirm the location of implanted electrode arrays, measure the depth of insertion and electrode position relative to vestibular nerve branches, and detect kinking, damage, or displacement. MR imaging is unsuitable for assessing electrode location because of field interactions that distort images and can displace the magnet of the implant, poor air-bone contrast within the temporal bone, and the inability of MR imaging to directly image the platinum/iridium wires and silicone that make up electrode arrays (other than by imaging displacement of inner ear fluids). Multislice CT (MSCT) is the better technique for characterizing cochlear implant position and is the current de facto standard, given its greater spatial resolution and better contrast among bone, air, metal, and fluid.<sup>6,7</sup> Metal artifacts, however, can significantly degrade image quality. Flat panel CT (FPCT), a relatively new imaging technique that yields tomographic reconstructions from images acquired using a C-arm x-ray system with flat panel image detectors, provides excellent visualization of high-contrast structures with better spatial resolution than MSCT.<sup>8,9</sup> In particular, FPCT produces images with sufficient resolution to precisely quantify cochlear electrode contact locations in a clinical setting.<sup>6,7,9,10</sup>

The purpose of this study was to present the very first imaging results of CT in vestibular implant imaging. In this report,

we present the technical aspects and imaging performance of MSCT and FPCT in assessing the intravestibular position of implanted electrode arrays in 8 participants in the first-in-human Multichannel Vestibular Implant Early Feasibility Study (clinicaltrials.gov, NCT02725463), and we suggest important features that should be reported in post-vestibular implantation imaging studies as well as a protocol for FPCT imaging of vestibular implants.<sup>11</sup>

## MATERIALS AND METHODS

This study was conducted under a protocol approved by the Johns Hopkins institutional review board (No. NA\_00051349) and was registered on the clinicaltrials.gov data base (NCT02725463).

### Vestibular Implant Electrode Array Design and Implantation

The implanted stimulator component of the Multichannel Vestibular Implant System (MVI; Labyrinth Devices) is a CONCERTO cochlear implant stimulator (MED-EL), modified for implantation in the SCCs (Fig 1A). It includes an electrode array with stimulation electrodes, a stimulation return and recording reference electrode, hermetically encapsulated electronics, 3 magnets, and an antenna coil for transcutaneous inductive transmission of power and control signals that the implant receives from the external system component.

The MVI is implanted via a postauricular incision and transmastoid approach similar to that typically used for cochlear implantation or labyrinthectomy, except that no entry is made into the cochlea and the SCCs are identified but not destroyed. Instead openings are made into the labyrinth for electrode array insertion (in the superior SCC ampulla, horizontal SCC ampulla, posterior SCC thin segment, and near the common crus). The electrode array (Fig 1B, C, and D) consists of a silicone carrier and comprises 10 platinum/iridium electrodes: 2 linear arrays of 3 electrodes each, joined to form a forked array inserted into the horizontal and superior ampullae; 3 on a linear array implanted in the posterior canal; and a braided platinum/iridium wire reference/return electrode inserted either into the common crus or in a subperiosteal pocket outside the temporal bone. Electrodes are spaced 0.2 mm apart in the silicone carrier for the forked array for the horizontal and

**Table 1: Demographic information for participants with vestibular implants**

Participants	Date Implanted	Date Imaged	Age (yr), <sup>a</sup> Sex	Imaging Protocol	Implant Side	Reference Location
1	12 Aug 2016	Sep 2016	62, M	MSCT	Left	CC
2	4 Nov 2016	Nov 2016	57, M	MSCT	Left	CC
3	3 Feb 2017	Feb 2017	63, F	FPCT, HR mode	Left	CC
4	15 Dec 2017	Jan 2018	62, F	FPCT, FF mode	Left	CC
5	24 Aug 2018	Sep 2018	51, F	FPCT, HR mode	Right	CC
6	31 Aug 2018	Sep 2018	66, F	FPCT, FF mode	Right	CC
7	14 Jan 2019	Feb 2019	53, F	FPCT, HR mode	Left	CC
8	13 Sep 2019	Oct 2019	55, M	FPCT, HR mode	Right	SP

**Note:**—CC indicates common crus of the implanted labyrinth; SP, in a subperiosteal pocket outside the temporal bone; Aug, August; Jan, January; Sep, September; Dec, December; Feb, February; Nov, November.

<sup>a</sup> Age in years at time of implantation.

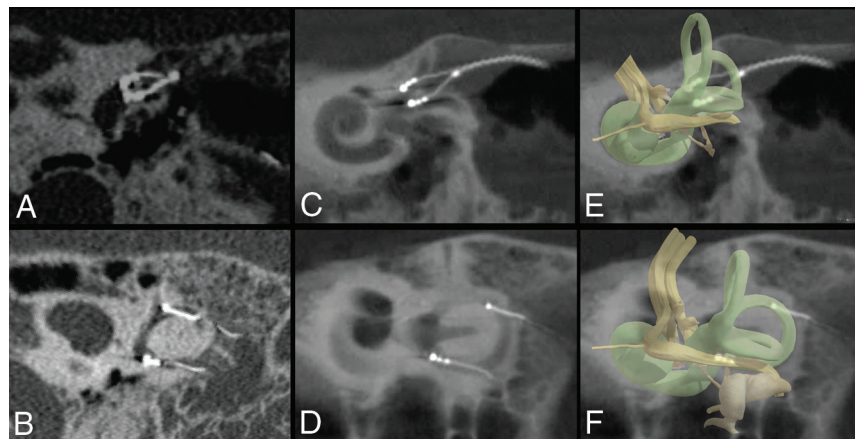


**FIG 2.** Method for generating MSCT (A and B) and FPCT (C and D) MPR. Two planes are generated. The first plane is approximately tangential to the thin segments of the superior and horizontal SCCs at their junctions with their ampullae and includes the 6 electrode contacts of the forked array inserted into the superior and horizontal ampullae. The second plane is in the posterior plane of the SCC and includes the 3 electrode contacts of the linear array implanted in the posterior canal and the tip of braided platinum/iridium wire inserted into the common crus. Section thickness was set to 2 mm to include all electrode contacts on 1 image for both planes. Window width and contrast level were adjusted as needed to optimize the visibility of electrode contacts. A 3D representation of the vestibular lumen and vestibular nerve is added in transparency (E and F) to help visualize the anatomy.

superior ampullae and 0.3 mm apart in the silicone carrier for the posterior SCC.

### Participants

Eight participants (3 men, 5 women; median age, 59.5 years, range, 51–66 years) disabled by bilateral vestibular hypofunction were implanted unilaterally with the implanted receiver/stimulator of the MVI. Three participants were implanted in the right ear, and 5 participants, in the left ear. Table 1 summarizes demographic information.

### Image Acquisition

After implantation, all subjects were scanned with either an MSCT (Somatom Sensation; Siemens) or a C-arm-based FPCT platform (Artis zee biplane; Siemens). MSCT was performed using standard clinical imaging parameters for temporal bone CT, with orientation of “axial” slices pitched to align with a plane through the horizontal SCC. Scanning was performed with 0.6-mm collimation, 120 kV, and 320 mAs. FPCT (DynaCT; Siemens) evaluation was performed using a flat panel angiography system (Axiom Artis zee;

Siemens) and commercially available software (syngo DynaCT; Siemens). The participant was placed supine on the angiography table, and the head was taped in place to limit participant motion. When we prepared the DynaCT acquisition, attention was paid to collimate the VOI to include only the temporal bones (craniocaudal collimation from just above the petrous ridges to just below the mastoid tip). A 20-second FPCT acquisition of the head was performed using the following parameters: 109 kV, small focus, 200° rotation angle, and angulation step of 0.4° per frame. FPCT was performed in 2 modes: full-field (FF) and high-resolution (HR). The FF mode uses top and bottom collimation, whereas the HR mode has collimation in all planes, allowing focal acquisition of the temporal bone of interest. Four participants underwent FPCT imaging with the HR mode, and 2 participants, with the FF mode.

### Reconstruction Parameters

The MSCT dataset was reformatted with 0.6-mm slices every 0.2 mm using a 512 × 512 matrix and a 65–70 mm FOV. FPCT secondary reconstructions were created with the following parameters: manually generated VOI to include only the electrode array; isotropic voxel size, 0.08 mm; 512 × 512 section matrix; sharp image characteristics.

### Multiplanar Images

We used MPR to generate 2 oblique 2D images. The first image was in the plane of the posterior SCC and included the 3 electrode contacts of the linear array implanted in the posterior canal and the tip of the braided platinum/iridium wire reference electrode inserted into the common crus. The second image was in a plane that was approximately tangential to the thin segments of the superior and horizontal canals and their junctions with their respective ampullae. This second image included the 6 electrode contacts of the forked array inserted into the superior and horizontal ampullae. Section thickness was set to 2 mm to include all

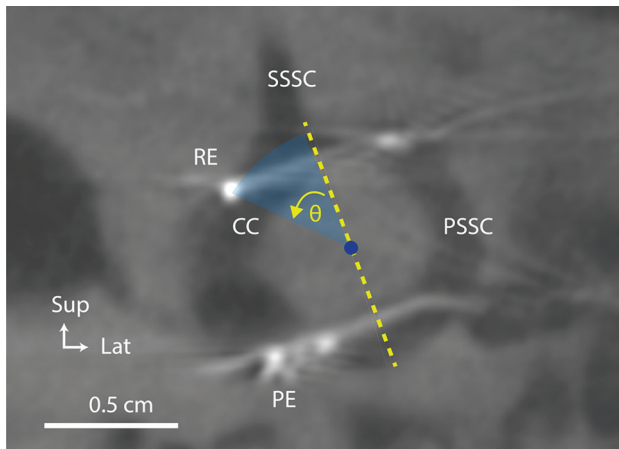


**FIG 3.** Subject: Participant 7. Method for calculating the angle ( $\theta$ ) of the angular insertion depth of the common crus reference electrode. CC indicates common crus of the implanted labyrinth; PE, posterior electrode array; PSSC, posterior semicircular canal; SSCC, superior semicircular canal; RE, reference electrode; Sup, superior; Lat, lateral.

electrode contacts on 1 image. Window width and contrast level were adjusted as needed to optimize the visibility of the electrode contacts (Fig 2).

### Measuring Common Crus Reference Electrode Insertion Depth

To see the tip of the braided platinum/iridium wire reference electrode inserted into the common crus, we reduced the MPR section thickness to 0.1 mm for an oblique section in the plane of the posterior canal. The crest of bone at the junction of the common crus, superior canal, and posterior canal was designated as the first reference point for measuring angular insertion depth of the reference electrode. A line drawn from the first reference point to the center of the circle formed by the posterior canal served as the reference (zero degree) line. The angle between the line joining the tip of the reference electrode and the center of the posterior SCC and the reference line was then calculated (Fig 3) and defined as the insertion depth angle. The angle was positive when the reference electrode tip was inserted deeper than the junction of the superior and posterior canal (deep insertion) and negative otherwise (short insertion). We also reported the length inserted by measuring the wire distance from the point of insertion in the posterior SCC to the tip of the reference electrode. All measures were individually performed by 2 radiologists; the mean result was obtained and reported if measures did not exceed a 10% error.

### Visualization of Electrode Contacts

Vestibular implant electrode array and single-electrode contacts were rated on a 3-point scale (0 = not visible; 1 = blurred, no single electrodes distinguishable; and 2 = clearly visible with single electrodes distinguishable).

## RESULTS

### Visualization of Individual Electrode Contacts

Individual electrode contacts were barely discernible in the 2 participants imaged using MSCT. Contacts and osseous structures were

detectable but blurred enough so that only 12 of the 18 stimulation electrode contacts could be individually identified (not visible,  $n = 0$ ; blurred,  $n = 6$ ; clearly visible,  $n = 12$ ). A blooming-type artifact (Fig 2A), in which the electrode array appears larger than its actual size, was identified on the MSCT images both between contacts and at the level of individual electrode contacts. Electrode arrays appeared to occupy most of the ampullae space, making it challenging to identify precisely each electrode contact.

FPCT was able to identify individually all 9 stimulating electrode contacts of the MVI arrays in all 6 participants, as well as all 6 reference electrodes inserted in the common crus (not visible,  $n = 0$ ; blurred,  $n = 0$ ; clearly visible,  $n = 60$ ). A linear sunburst streak artifact (Fig 2C) was observed in all FPCT images and was noticeable at the level of individual electrode contacts but was reduced between electrode contacts. The use of the HR mode when obtaining FPCT images ( $n = 4$  participants) produced the clearest images of the electrode array and surrounding labyrinthine structures. After we used the FF mode ( $n = 2$  participants), all individual electrode contacts could be identified, but electrodes and surrounding osseous structures were less well-resolved compared with the HR mode. MPR reconstructions for all subjects are shown in Fig 4.

### Common Crus Insertion Depth

The median reference electrode insertion depth angle was  $9^\circ$  (range,  $-57.5^\circ$  to  $45^\circ$ ). The median reference electrode insertion length was 42 mm (range, 21–66 mm). The reference electrode tip was within the common crus in 3 participants, in the superior canal proximal to the common crus in 1 patient, in the posterior canal in 3 participants, and in a subperiosteal pocket in one. Results are summarized in Table 2.

## DISCUSSION

Accurately positioning each electrode array near the nerve branch of the SCCs that it is intended to stimulate can maximize the strength and selectivity of the prosthetic stimulation because it reduces the current intensity required to achieve and excite a given proportion of neurons in the targeted nerve branch and also reduces current spread to adjacent neurons in other vestibular nerve branches. Vestibular implant outcomes can vary considerably depending on the strength and selectivity of the electrode-nerve interface, as indicated by variation in the magnitude and direction of reflex eye movements driven by stimuli meant to target each nerve branch individually.<sup>4</sup> Electrode distances to target and nontarget nerve branches are key determinants of the strength and selectivity of stimulation; changing electrode location by  $\sim 200$   $\mu\text{m}$  can change implant outcomes dramatically. Typically, 1 electrode on an electrode array of a given canal outperforms the others that are 250–500  $\mu\text{m}$  away.<sup>12</sup>

Knowing vestibular implant array location, their insertion depth, and distance from target vestibular nerve branches can provide helpful information to choose the best electrodes to activate and define stimulus parameters to use, valuable insights that can drive iterative improvements in electrode array design and surgical technique. For example, electrode contact locations can be used as input to individualized finite element models that, once adequately validated via comparison with real data, can facilitate interpretation of empiric data, generation of testable

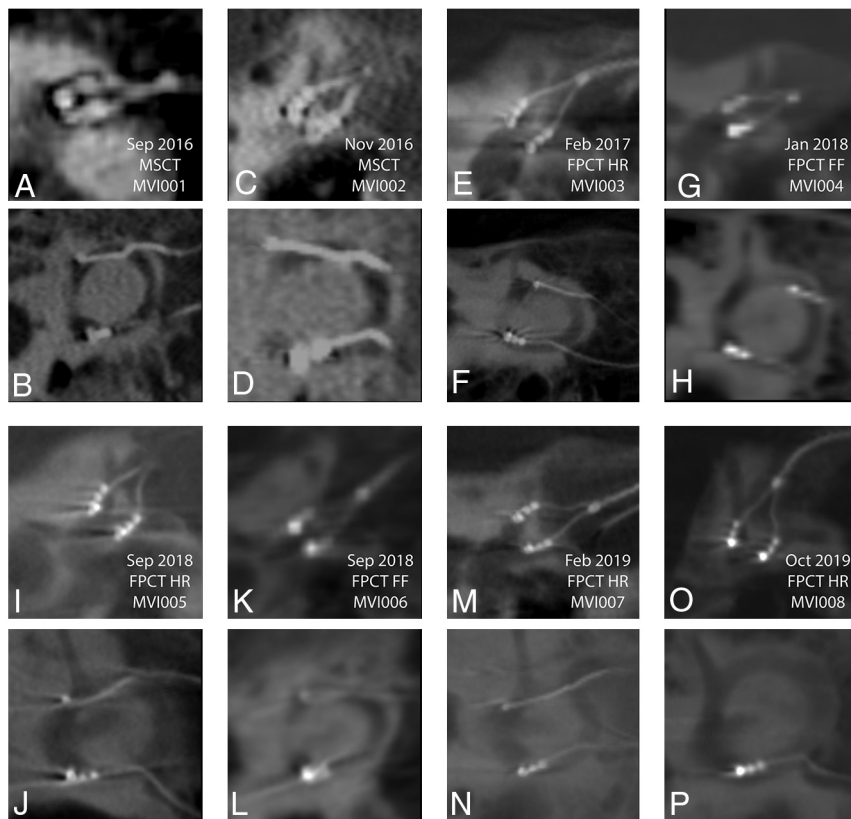


**FIG 4.** MSCT (A–D) and FPCT (E–P) multiplanar reconstructions for all participants. A and B, Participant 1 MSCT. C and D, Participant 2 MSCT. E and F, Participant 3 FPCT. G and H, Participant 4 FPCT. I and J, Participant 5 FPCT. K and L, Participant 6 FPCT, M and N, Participant 7 FPCT. O and P, Participant 8 FPCT. In every panel, the top of the image is superior and the left edge of the image is anteromedial. Sep indicates September; Feb, February; Oct, October; Nov, November; Jan, January.

**Table 2: Common crus reference electrode angular depth and insertion length calculations and locations**

Participant No.	CC Insertion Intended	Insertion Depth Angle	Insertion Length (mm)	Anatomic Location of the Reference Electrode Tip
1	Yes	−3°	39	Common crus
2	Yes	+26°	66	Superior canal
3	Yes	−30°	42	Posterior canal
4	Yes	−57°	21	Posterior canal
5	Yes	+21°	46	Common crus
6	Yes	−2°	41	Posterior canal
7	Yes	+45°	51	Common crus
8	No	NA	NA	Outside temporal bone

**Note:**—NA indicates not applicable.

hypotheses, and optimization of electrode array designs through simulation.<sup>12</sup>

In the present study, we found that the locations of stimulating electrodes and their relation to vestibular bony structures can be depicted precisely with FPCT. All stimulating electrode arrays were close to their target end organs within the target ampullae; however, they varied with respect to location: adjacent to or far from the bone walls of each ampulla. Electrode contact with vestibular labyrinth walls may influence electrode impedance and the spatial pattern of current density, altering stimulation efficiency and

selectivity. We also found that reference electrode location varied significantly from case to case, likely because the surgical technique used (making as small an entry as possible in the posterior canal near the common crus, then sliding the reference electrode in with the intent of it reaching the common crus) does not permit direct intraoperative observation or steering of the electrode tip. In 2 cases, the reference electrode was inserted into the superior SCC instead of going down through the common crus. Intraoperative fluoroscopy or DynaCT may be helpful for guiding or confirming the electrode location.

### FPCT versus MSCT

FPCT is a relatively new imaging technology that implements flat detectors to create volumetric reconstructions. Several advantages have been seen in angiography and temporal bone imaging for cochlear implantation.<sup>13</sup> FPCT is a rapid imaging technique that obtains a full dataset of temporal bone images in approximately 20 seconds. The most clinically significant advantage of FPCT over MSCT is the ability for small voxel areas to be viewed with high resolution. Due to its higher spatial resolution, FPCT yields equal or higher image quality than MSCT when assessing bony structures of diagnostic interest for radiologists.<sup>7,8,14-16</sup> Potential drawbacks to using FPCT for temporal bone imaging compared with MSCT include lack of widespread availability and poorer resolution of soft tissue with currently available FPCT systems.

A significant reduction in artifacts was appreciated on FPCT images over MSCT images. A blooming artifact, with the electrode array appearing larger than its actual size, was identified on the MSCT images. This smooth,

concentric artifact was identified both between and at the level of the individual electrode contacts, making it challenging to identify precisely each electrode contact. A beam artifact (linear streak bands) was noticeable on the FPCT images at the level of individual electrode contacts but was significantly reduced between electrode contacts. The position of the electrode contacts was better assessed on the FPCT images mainly because of the decrease in artifacts between them.

Previous authors have reported that an important advantage of FPCT is a reduced radiation dose compared with standard

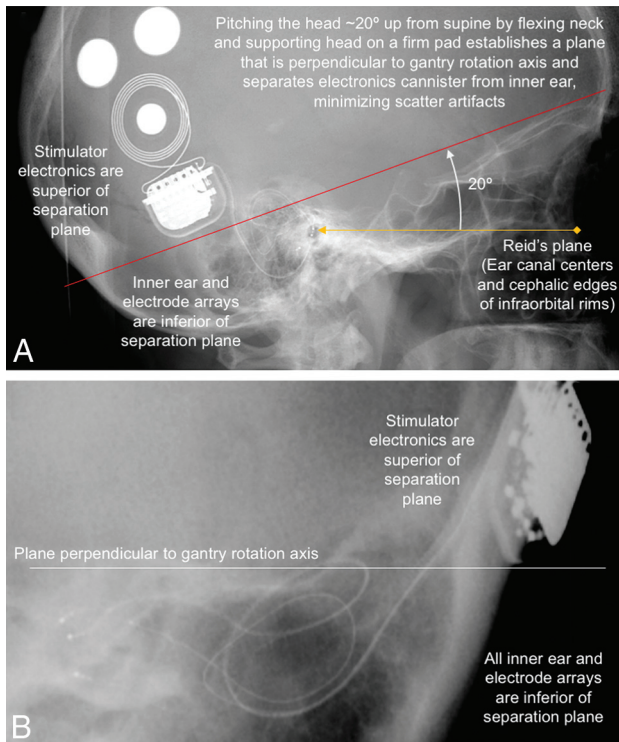


**FIG 5.** A, Lateral scout view showing electrode arrays visible through the external auditory canals (*yellow arrowhead*) and cephalic edges of the infraorbital rims (*yellow diamond*). Those palpable landmarks define the Reid plane (*yellow line*) and the plane of horizontal canals (*red line*). The plane of the horizontal semicircular canals, the standard “axial” plane for temporal bone CT reconstructions, is at a  $\sim 20^\circ$  pitch from the Reid plane.<sup>17</sup> By supporting the head on a firm wedge to pitch the head forward from supine (and flexing the neck until the Reid plane is pitched  $\sim 20^\circ$  nose toward chest from Earth vertical), one can minimize scatter artifacts from the stimulator cannister to the inner ear by keeping them on opposite sides of a separation plane perpendicular to the gantry rotation axis (B).

temporal bone MSCT protocols.<sup>8</sup> Depending on the clinical question, FPCT can reduce the radiation dose even more by imaging only the implanted ear. The collimation available in HR mode can direct the x-ray beam to the ear of interest, minimizing the dose received by the head.

### Protocol for Vestibular Implant Imaging

Similar to imaging after cochlear implantation,<sup>7,9</sup> FPCT imaging of postoperative vestibular implantation is easy to perform, produces high-resolution images, and can depict all individual electrode contacts. Patients should be positioned supine with the head pitched to prevent shadowing/overlap of the stimulator and/or magnets with the inner ear. Our imaging methods use a high-resolution secondary reconstruction algorithm with a manually generated small VOI (voxel size = 0.08 mm), Hounsfield unit kernel type, and sharp image characteristic. A 20-second FPCT acquisition of the head is performed using the following parameters: 109 kV, small focus,  $200^\circ$  rotation angle, and  $0.4^\circ$  per frame angulation step. Before image acquisition, the external components of the vestibular implant system are removed. The patient’s head is pitched forward  $\sim 20^\circ$  by flexing the neck and

supporting the head on a firm wedge. The head is then taped in place. This positioning ensures that the Reid plane (which contains the center of the external auditory canals and the cephalic edges of the infraorbital rims, both easily palpable landmarks) is pitched  $\sim 20^\circ$  from Earth-vertical, so that the horizontal SCC plane is approximately perpendicular to the gantry rotation axis and scatter artifacts from the magnets and stimulator electronics will not shadow the inner ear (Fig 5). Acquisition should include the entire implant, overlying scalp (to check scalp thickness over the magnets), inner ears, and at least the maxillary teeth (which are used to get canal orientation relative to a bite block for programming the alignment matrix of the processor).

Finally, multiplanar reconstructions are performed in the axial (horizontal plane of the SCC) and coronal planes, the planes of the superior and posterior canals (which also gives slices through the basal turn of the cochlea), and the plane that contains the superior and horizontal forked electrode array. This last plane should be tangential to the superior and horizontal canals at the junction of their ampullae as described in the Materials and Methods above. When reporting imaging findings of FPCT, we recommend that in addition to commenting on common temporal bone imaging findings, additional comments should be made on the quality of the examination, the number of metallic artifacts, the locations of stimulating electrode contacts relative to the ampullae, the location of the tip of the reference electrode if applicable; and scalp thickness over the implant.

This study has some limitations including a small sample size, lack of a control group, and lack of clinical information regarding correlation between vestibular function recovery and electrode contact positions. These topics are beyond the scope of this article, which aims to present the very first imaging results that are currently under investigation to be addressed in future studies in which imaging plays an important role.

Future development of vestibular imaging may lead to intraoperative DynaCT. DynaCT technology can be applied with acceptable additional time requirements without adding too much complexity to the surgical procedure. Intraoperative data acquisition by DynaCT may represent a suitable option for real-time surgical navigation during a vestibular implant operation. This imaging technology will encourage further advances in vestibular implant surgery and integrate functional aspects of imaging by applying individualized anatomy-based mathematic models that will help predict vestibular flow current spreading for each patient to further understand clinical outcomes of prosthesis implantation.

### CONCLUSIONS

FPCT produces high-resolution images of vestibular implants, allowing identification of individual electrode contacts and quantification of their locations relative to vestibular SCC ampullae. Reduced artifacts were seen in FPCT images compared with MSCT images. Optimal FPCT imaging includes a high-resolution secondary reconstruction algorithm with a manually generated VOI that includes only the electrode array. As MVI imaging improves, so will our understanding of the relationships among vestibular anatomy, MVI electrode placement, vestibular performance, and hearing outcomes.

## ACKNOWLEDGMENTS

We thank the 8 pioneering study subjects whose CT images are shown in this report; engineers on the MED-EL Vestibular Implant Systems team; Johns Hopkins School of Medicine trainees, faculty, and staff who facilitated this work; and members of the Data and Safety Monitoring Board (Drs David Eisenman, Frank Lin, and Charles Matthew Stewart).

Disclosures: Abderrahmane Hedjoudje—*RELATED: Grant:* National Institute on Deafness and Other Communication Disorders R01DC013536 and 2T32DC000023, Labyrinth Devices, and MED-EL.\* Desi P. Schoo—*RELATED: Grant:* National Institutes of Health, *Comments:* My work/effort during this project was funded, in part, by the National Institutes of Health training grant Research Training in Otolaryngology (5T32DC000027-30)\*; *Support for Travel to Meetings for the Study or Other Purposes:* MED-EL, *Comments:* MED-EL provided funding for expenses related to travel and lodging for the following meetings. 1) Implantable Vestibular Prosthesis Meeting, Innsbruck and Vienna, Austria, March 2017; 2) The 16th Hearing and Structure Preservation Workshop, Perth, Australia, November 2017; *UNRELATED: Employment:* Johns Hopkins Hospital, *Comments:* Resident Physician in the Department of Otolaryngology-Head and Neck Surgery, Bryan K. Ward—*RELATED: Grant:* American Otological Society, *Comments:* Clinician Scientist Award\*; *UNRELATED: Patents (Planned, Pending or Issued):* US 20180036549 A1, *Comments:* device for magnetic stimulation of the vestibular system\*; *Payment for Development of Educational Presentations:* practical reviews, *Comments:* critically review recently-published studies in otolaryngology-head and neck surgery. John P. Carey—*RELATED: Grant:* National Institutes of Health\*; *Support for Travel to Meetings for the Study or Other Purposes:* Med-EL, *Comments:* MED-EL reimbursed me for 1 meeting in Austria to discuss this study and other ongoing vestibular implant studies; *UNRELATED: Grants/Grants Pending:* National Institutes of Health. Charles C. Della Santina—*RELATED: Grant:* Labyrinth Devices, MED-EL, *Comments:* 1) clinical trial agreement between Labyrinth Devices and Johns Hopkins University, 2) research contract between MED-EL and Johns Hopkins University\*; *Support for Travel to Meetings for the Study or Other Purposes:* MED-EL, *Comments:* travel support to investigator meeting; *Provision of Writing Assistance, Medicines, Equipment, or Administrative Support:* Labyrinth Devices, MED-EL, *Comments:* provision of equipment and devices for use in research\*; *UNRELATED: Grants/Grants Pending:* Labyrinth Devices, MED-EL, *Comments:* 1) clinical trial agreement between Labyrinth Devices and Johns Hopkins University, 2) research contract between MED-EL and Johns Hopkins University\*; *Patents (Planned, Pending or Issued):* System For Synchronously Sampled Binocular Video-Oculography Using A Single Head-Mounted Camera Publication number: 20150223683\*; *Other:* Labyrinth Devices, *Comments:* equity, spouse employed part-time as administrator. \*Money paid to the institution.

## REFERENCES

1. LIVING without a balancing mechanism. *N Engl J Med* 1952;246:458–60 [CrossRef Medline](#)
2. Ward BK, Agrawal Y, Hoffman HJ, et al. Prevalence and impact of bilateral vestibular hypofunction. *JAMA Otolaryngol Head Neck Surg* 2013;139:803–10 [CrossRef Medline](#)
3. Sun DQ, Ward BK, Semenov YR, et al. Bilateral vestibular deficiency: quality of life and economic implications. *JAMA Otolaryngol Head Neck Surg* 2014;140:527 [CrossRef Medline](#)
4. Boutros PJ, Schoo DP, Rahman M, et al. Continuous vestibular implant stimulation partially restores eye-stabilizing reflexes. *JCI Insight* 2019;4:e128397 [CrossRef Medline](#)
5. Sluydts M, Curthoys I, Vanspauwen R, et al. Electrical vestibular stimulation in humans: a narrative review. *Audiol Neurootol* 2020;25:6–24 [CrossRef Medline](#)
6. Jiam NT, Jiradejvong P, Pearl MS, et al. The effect of round window vs cochleostomy surgical approaches on cochlear implant electrode position a flat-panel computed tomography study. *JAMA Otolaryngol Head Neck Surg* 2016;142:873–80 [CrossRef Medline](#)
7. Jiam NT, Pearl MS, Carver C, et al. Flat-panel CT imaging for individualized pitch mapping in cochlear implant users. *Otol Neurotol* 2016;37:672–79 [CrossRef Medline](#)
8. Piergallini L, Scola E, Tuscano B, et al. Flat-panel CT versus 128-slice CT in temporal bone imaging: assessment of image quality and radiation dose. *Eur J Radiol* 2018;106:106–13 [CrossRef Medline](#)
9. Pearl MS, Roy A, Limb CJ. High-resolution secondary reconstructions with the use of flat panel CT in the clinical assessment of patients with cochlear implants. *AJNR Am J Neuroradiol* 2014;35:1202–08 [CrossRef Medline](#)
10. Roy AT, Penninger RT, Pearl MS, et al. Deeper cochlear implant electrode insertion angle improves detection of musical sound quality deterioration related to bass frequency removal. *Otol Neurotol* 2016;37:146–51 [CrossRef Medline](#)
11. Multichannel Vestibular Implant Early Feasibility Study. <https://clinicaltrials.gov/ct2/show/NCT02725463>. Accessed April 01, 2016
12. Hedjoudje A, Hayden R, Dai C, et al. Virtual Rhesus Labyrinth Model predicts responses to electrical stimulation delivered by a vestibular prosthesis. *J Assoc Res Otolaryngol* 2019;20:313–39 [CrossRef Medline](#)
13. Tunkel AE, Carey JP, Pearl M. Flat panel computed tomography in the diagnosis of superior semicircular canal dehiscence syndrome. *Otol Neurotol* 2019;40:213–17 [CrossRef Medline](#)
14. Liao D, Pearl MS, Ward BK. Flat-panel CT imaging of a radiopaque shim for patulous eustachian tube dysfunction. *Otol Neurotol* 2020;41:e412–13 [CrossRef Medline](#)
15. Mekabaty AE, Pross SE, Martinez M, et al. Reducing radiation dose for high-resolution flat-panel CT imaging of superior semicircular canal dehiscence. *Otol Neurotol* 2018;39:e683–90 [CrossRef Medline](#)
16. Kennedy TA, Connell N, Szczykutowicz T, et al. Flat-panel CT for cochlear implant electrode imaging: comparison to multi-detector CT. *Otol Neurotol* 2016;37:1646–53 [CrossRef Medline](#)
17. Della Santina CC, Potyagaylo V, Migliaccio AA, et al. Orientation of human semicircular canals measured by three-dimensional multiplanar CT reconstruction. *J Assoc Res Otolaryngol* 2005;6:191–206 [CrossRef Medline](#)